Electron-ion radiative recombination assisted by a bichromatic elliptically polarized laser field

A. Čerkić,[1] M. Busuladžić,[2,1] and D. B. Milošević[1,3,4]

[1]*Faculty of Science, University of Sarajevo, Zmaja od Bosne 35, 71000 Sarajevo, Bosnia and Herzegovina*

[2]*Faculty of Medicine, University of Sarajevo, Čekaluša 90, 71000 Sarajevo, Bosnia and Herzegovina*

[3]*Academy of Sciences and Arts of Bosnia and Herzegovina, Bistrik 7, 71000 Sarajevo, Bosnia and Herzegovina*

[4]*Max-Born-Institut, Max-Born-Straße 2A, 12489 Berlin, Germany*

(Received 24 February 2017; revised manuscript received 8 May 2017; published 1 June 2017)

Electron-ion radiative recombination assisted by a bichromatic (two-component) elliptically polarized laser field is analyzed in the frame of the S-matrix theory. The second Born approximation is applied in the expansion of the S-matrix element where the first term in the expansion corresponds to the direct recombination of electrons with ionic targets, while the second term corresponds to the recombination preceded by an electron-ion scattering. The latter process is possible in the presence of a laser field. If the electron scatters on an ionic target, it may be subsequently driven back by the laser field and recombine with the same ion. The photon emitted in this process may have a high energy. We have studied the dependence of the energy spectrum on various laser-field and incident electron parameters. The energy spectra obtained show plateaulike structures with abrupt cutoffs. These cutoffs are explained by a classical analysis.

DOI: 10.1103/PhysRevA.95.063401

I. INTRODUCTION

Processes involving the interaction of a strong laser field with matter have been intensively studied over the past few decades [1–3]. Particularly interesting are the processes that generate soft x rays, i.e., high-energy photons. Examples of these processes are high-order-harmonic generation [4,5] (see also the review articles [6–9] and references therein), laser-induced bremsstrahlung [10–15], laser-assisted x-ray–atom scattering [16–18], and laser-assisted electron-ion recombination (LAR) [19,20].

Electron-ion recombination is a very important process, especially in plasma physics and astrophysics [21]. A special case of this process is radiative recombination, where the energy is transferred from the free electron to a photon. If the process occurs in a laser field, the incident electron may exchange energy with the laser field before it recombines with the target ion. This may result in the emission of a high-energy photon. More specifically, the process is described as follows: The incident electron having momentum $\mathbf{p}$ and energy $E_{\mathbf{p}} = \mathbf{p}^2/2$ recombines with a positive ion and an atomic bound state $|\psi_{\mathrm{B}}\rangle$ having energy $E_{\mathrm{B}} < 0$ is formed. This process happens in the presence of a strong periodic laser field with the electric-field vector $\mathbf{E}(t)$ and is denoted by LAR. The result is the emission of an x-ray photon having the wave vector $\mathbf{K}$, frequency $\omega_{\mathbf{K}}$, and unit complex polarization vector $\hat{\mathbf{e}}_{\mathbf{K}}$, while n photons are exchanged with the laser field. The energy-conserving condition for this process is $n\omega = \omega_{\mathbf{K}} + E_{\mathrm{B}} - E_{\mathbf{p}} - U_{\mathrm{p}}$, where $U_{\mathrm{p}} = \int_0^T dt\, \mathbf{A}^2(t)/2T$ is the ponderomotive energy, with $\mathbf{A}(t) = -\int^t dt' \mathbf{E}(t')$ and T the period of the laser field.

The incident electron may also scatter on an ion instead of recombining with it. It is then possible that the scattered electron, driven by the laser field, returns to the same ion and recombines with it. This process is referred to as recombination preceded by a scattering (SLAR). The probability of the SLAR process is considerably lower than that of the LAR process. On the other hand, the photons emitted in the SLAR process may have higher energies than those emitted in the LAR process.

The LAR process in infinitely long, linearly polarized laser pulses was analyzed in Refs. [19,20,22–24] (monochromatic field) and Ref. [25] (bichromatic field), while the same process in a bicircular laser field was considered in Ref. [26]. The LAR process in few-cycle laser pulses was investigated in Refs. [27–29]. The improved theories of laser-assisted electron-ion recombination that include the scattering effects (SLAR) were presented in Refs. [30–32] for infinitely long, linearly polarized laser pulses and in Ref. [33] for few-cycle laser pulses. In order to obtain the recombination energy spectra, the S-matrix approach was applied in Refs. [30,33], while the time-dependent effective range theory in quasienergy-state formalism was used in Refs. [14,31,32].

Experimental data on laser-assisted recombination are sparse because a three-beam experiment must be performed to obtain the process. In such an experiment, three beams (the ionic target, electron, and laser beams) must be crossed in coincidence and the emitted photons are recorded. These experiments are difficult to realize as the counting rates are very low. Some recent experimental findings on electron-ion recombination were presented in Refs. [34,35]. The phase-dependent electron-ion recombination was observed in Ref. [34], while the polarization dependence of electron–D^+-ion recombination was investigated in Ref. [35]. The presence of an external laser field may considerably increase the recombination yield. These laser-induced enhancements of the recombination rate have been observed in experiments with merged ion and electron beams (in ion storage rings) [36] and they can be important for the laser-assisted neutral antimatter formation [37]. We also mention recent investigation of the effect of bound-state dressing in LAR [38] and work on radiative recombination of twisted electrons with bare nuclei [39].

In this paper we analyze the electron-ion radiative recombination in a bichromatic elliptically polarized laser field as a second-order process (i.e., both LAR and SLAR are included). The quantum-mechanical theory based on the S-matrix formalism is given in Sec. II, our classical analysis is described in Sec. III, and the numerical results are presented

in Sec. IV. The conclusions are summarized in Sec. V. We use the atomic system of units ($\hbar = e = m_e = 4\pi\varepsilon_0 = 1$).

II. QUANTUM-MECHANICAL THEORY

A comprehensive theoretical description of the laser-assisted electron-ion radiative recombination, based on the S-matrix formalism, was given in [7,30]. We present here the basic steps. The general form of the S matrix is

$$S_{\rm fi} = i \lim_{\substack{t' \to \infty \\ t \to -\infty}} \langle \Phi_{\rm out}(t') | G(t',t) | \Phi_{\rm in}(t) \rangle, \tag{1}$$

where $G \equiv G^{(+)}$ is the total retarded time-dependent Green's operator that corresponds to the total Hamiltonian. In our case, the total Hamiltonian is given by

$$H(t) = H_0(t) + V_{\rm X}(\mathbf{r},t), \quad H_0(t) = -\frac{\nabla^2}{2} + V(\mathbf{r}) + V_{\rm L}(t), \tag{2}$$

where $\boldsymbol{\nabla} \equiv \partial/\partial\mathbf{r}$, $V(\mathbf{r})$ is the atomic binding potential, $V_{\rm L}(t)$ is the laser-atom interaction, and $V_{\rm X}(\mathbf{r},t)$ is the interaction of the atom with the x-ray field. We use the length gauge and apply the dipole approximation to the laser field, so $V_{\rm L}(t) = \mathbf{r}\cdot\mathbf{E}(t)$ and $V_{\rm X}(\mathbf{r},t) = \mathbf{r}\cdot\mathbf{E}_{\rm X}(\mathbf{r},t)$, where $\mathbf{E}(t)$ and $\mathbf{E}_{\rm X}(\mathbf{r},t)$ are the electric-field vectors of the laser field and x-ray radiation, respectively. The x-ray radiation field is quantized, so

$$\mathbf{E}_{\rm X}(\mathbf{r},t) = \mathbf{E}_{\rm X}^{(+)}(\mathbf{r},t) + \mathbf{E}_{\rm X}^{(-)}(\mathbf{r},t), \tag{3}$$

$$\mathbf{E}_{\rm X}^{(+)}(\mathbf{r},t) = i C_{\mathbf{K}} \hat{\mathbf{e}}_{\mathbf{K}} a_{\mathbf{K}} e^{-i(\omega_{\mathbf{K}} t - \mathbf{K}\cdot\mathbf{r})}, \tag{4}$$

$$\mathbf{E}_{\rm X}^{(-)}(\mathbf{r},t) = -i C_{\mathbf{K}} \hat{\mathbf{e}}_{\mathbf{K}} a_{\mathbf{K}}^{\dagger} e^{i(\omega_{\mathbf{K}} t - \mathbf{K}\cdot\mathbf{r})}, \tag{5}$$

where $a_{\mathbf{K}}$ and $a_{\mathbf{K}}^{\dagger}$ are the photon annihilation and creation operators of the x-ray field, respectively, and $C_{\mathbf{K}}^2 = 2\pi\omega_{\mathbf{K}}/\mathcal{V}$, with $\mathcal{V}$ representing the quantization volume.

After applying the second Born approximation in the expansion of the S-matrix element and approximating the scattering potential by a short-range potential, the S-matrix element may be written as

$$\begin{aligned} S_{\rm fi} = -C_{\mathbf{K}} \int_{-\infty}^{\infty} dt\, e^{i(E_{\rm B}+\omega_{\mathbf{K}})t} \Big\{ & \langle \psi_{\rm B} | \mathbf{r}\cdot\hat{\mathbf{e}}_{\mathbf{K}}^{*} e^{-i\mathbf{K}\cdot\mathbf{r}} | \chi_{\mathbf{p}}(t) \rangle \\ & - i \int_{-\infty}^{t} dt' \int d^3\mathbf{q} \langle \psi_{\rm B} | \mathbf{r}\cdot\hat{\mathbf{e}}_{\mathbf{K}}^{*} e^{-i\mathbf{K}\cdot\mathbf{r}} | \chi_{\mathbf{q}}(t) \rangle \\ & \times \langle \chi_{\mathbf{q}}(t') | V_{\rm S} | \chi_{\mathbf{p}}(t') \rangle \Big\}, \end{aligned} \tag{6}$$

where $E_{\rm B}$ and $\psi_{\rm B}$ are the energy and spatial wave function of the atomic bound state, respectively, $\mathbf{q}$ is the intermediate electron momentum, $V_{\rm S}$ is a short-range scattering potential, and $\chi_{\mathbf{p}}$ and $\chi_{\mathbf{q}}$ are the Volkov wave vectors in the length gauge. They are defined by

$$|\chi_{\mathbf{p}}(t)\rangle = |\mathbf{p} + \mathbf{A}(t)\rangle \exp\{-i[\mathbf{p}\cdot\boldsymbol{\alpha}(t) + \mathcal{U}(t) + E_{\mathbf{p}} t]\}, \tag{7}$$

where $\boldsymbol{\alpha}(t) = \int^t dt' \mathbf{A}(t')$ and

$$\mathcal{U}(t) = \frac{1}{2}\int^t dt' \mathbf{A}^2(t') = \mathcal{U}_1(t) + U_{\rm p} t, \tag{8}$$

with $\mathcal{U}_1(t)$ the time-periodic part of $\mathcal{U}(t)$. Incident electrons may be accelerated by the laser field, having high energies at the time of the collision with the targets, as we will illustrate in Sec. IV. Therefore, the Born approximation is applicable. The first term on the right-hand side of Eq. (6) corresponds to the LAR process (the direct recombination), while the second term describes the SLAR process (the recombination preceded by a scattering). Introducing the substitution $t' = t - \tau$, the integral over the scattering time t' in Eq. (6) is replaced by an integral over the travel time τ (i.e., the time between the scattering and the recombination). The next step is to solve the integral over intermediate electron momenta $\mathbf{q}$ by the saddle-point method [16,18,40,41]. This integral can be presented as a Taylor expansion around the saddle point $\mathbf{q} = \mathbf{k}_{\rm s}$ that contains powers of $1/\tau$ multiplied by the even derivatives of the subintegral function over the intermediate electron momenta. We suppose that $\tau \gg 1$, so the zeroth-order term in the expansion is dominant and all other terms may be neglected. In this way, the S-matrix element (6) becomes

$$\begin{aligned} S_{\rm fi} &= -C_{\mathbf{K}} \int_{-\infty}^{\infty} dt\, e^{i[(E_{\rm B}+\omega_{\mathbf{K}}-E_{\mathbf{p}}-U_{\rm p})t}\, \mathcal{T}_{\rm fi}(\omega t) \\ &= -2\pi C_{\mathbf{K}} \sum_n \delta(E_{\rm B} + \omega_{\mathbf{K}} - E_{\mathbf{p}} - U_{\rm p} - n\omega) T_{\rm fi}(n), \end{aligned} \tag{9}$$

where ω is the angular frequency of the laser field and

$$\begin{aligned} \mathcal{T}_{\rm fi}(\omega t) = e^{-i[\mathbf{p}\cdot\boldsymbol{\alpha}(t) + \mathcal{U}_1(t)]} \Big\{ & \langle \psi_{\rm B} | \mathbf{r}\cdot\hat{\mathbf{e}}_{\mathbf{K}}^{*} e^{-i\mathbf{K}\cdot\mathbf{r}} | \mathbf{p} + \mathbf{A}(t) \rangle \\ & - i \int_0^{\infty} d\tau \left(\frac{2\pi}{i\tau}\right)^{3/2} \langle \psi_{\rm B} | \mathbf{r}\cdot\hat{\mathbf{e}}_{\mathbf{K}}^{*} e^{-i\mathbf{K}\cdot\mathbf{r}} | \mathbf{k}_{\rm s} + \mathbf{A}(t) \rangle \\ & \times \langle \mathbf{k}_{\rm s} | V_{\rm S} | \mathbf{p} \rangle e^{i(\mathbf{p}-\mathbf{k}_{\rm s})^2 \tau/2} \Big\} = \sum_{n=-\infty}^{\infty} T_{\rm fi}(n) e^{-in\omega t}, \end{aligned} \tag{10}$$

$$T_{\rm fi}(n) = \int_0^T \frac{dt}{T} \mathcal{T}_{\rm fi}(\omega t) e^{in\omega t}, \tag{11}$$

with $\mathbf{k}_{\rm s} = [\boldsymbol{\alpha}(t-\tau) - \boldsymbol{\alpha}(t)]/\tau$ representing the stationary intermediate electron momentum and $T = 2\pi/\omega$ the laser-field period. In Eqs. (9)–(11), $T_{\rm fi}(n)$ and $\mathcal{T}_{\rm fi}(\omega t)$ are the T-matrix element and its Fourier transform, respectively. The δ function in Eq. (9) expresses the energy-conserving condition.

The differential rate for the emission of an x-ray photon having energy $\omega_{\mathbf{K}}$ into the solid angle $d\Omega_{\mathbf{K}}$, after the recombination of an electron having initial energy $E_{\mathbf{p}}$ and impinging from within the solid angle $d\Omega_{\mathbf{p}}$, is given by [30]

$$dw(\mathbf{K},\mathbf{p}) = \frac{p\omega_{\mathbf{K}}^3}{2\pi c^3} |T_{\rm fi}(n)|^2 d\Omega_{\mathbf{K}} d E_{\mathbf{p}} d\Omega_{\mathbf{p}}. \tag{12}$$

The differential power spectrum of the laser-assisted electron-ion radiative recombination is

$$S_n(\mathbf{K},\mathbf{p}) = \frac{\omega_{\mathbf{K}} dw(\mathbf{K},\mathbf{p})}{d\Omega_{\mathbf{K}} d E_{\mathbf{p}} d\Omega_{\mathbf{p}}} = \frac{p\omega_{\mathbf{K}}^4}{2\pi c^3} |T_n|^2, \tag{13}$$

with $T_n \equiv T_{\rm fi}(n)$.

A generalization of the theory to the N-electron atoms, which neglect the influence of the spin, can be obtained using

the Hartree-Fock approximation in which the final atomic bound state is presented as the product of the single-electron orbitals: $|\psi_{\rm B}(t)\rangle = \prod_{j=1}^{N} |\psi_{{\rm B}j}(t)\rangle$, where $\psi_{{\rm B}j}$ are modeled by a linear combination of the Slater orbitals $\psi_{n_a lm}(\mathbf{r}_j)$ [42]. We suppose that the jth electron is incident on the ion and, during recombination, a high-energy photon is emitted via the interaction $\hat{\mathbf{e}}^*_{\mathbf{K}} \cdot \mathbf{r}_j e^{-i\mathbf{K}\cdot\mathbf{r}_j}$. We consider atoms with closed shell having fixed orbital quantum number l ($l = m = 0$ for He and $l = 1$ and $m = 0, \pm 1$ for Ne, Ar, Kr, and Xe).

We define the averaged differential rate for the emission of an x-ray photon analogously as in [43], where we defined the averaged differential ionization rate for the above-threshold ionization process, which is an inverse process of the LAR. This definition includes summation over all values of $m = -l, \ldots, l$. Therefore, we define the averaged differential power spectrum $\overline{S}_n$, which is a generalization of the result from [26], by

$$\overline{S}_n(\mathbf{K},\mathbf{p}) = \frac{1}{2l+1} \frac{p\omega_{\mathbf{K}}^4}{2\pi c^3} \sum_{m=-l}^{l} |T_{m,n}|^2, \tag{14}$$

where $T_{m,n}$ is given by Eqs. (10) and (11), with $|\psi_{\rm B}\rangle \equiv |\psi_{{\rm B}m}\rangle$ the atomic bound state for a specific value of m. It is easy to show that $\overline{S}_n$ does not depend on the choice of the quantization axis. If we choose the z axis as the axis of quantization, then the atomic wave function is expressed via spherical harmonics $Y_{lm}(\hat{\mathbf{r}})$, $\psi_{{\rm B}m} = R_{\rm B}(r) Y_{lm}(\hat{\mathbf{r}})$. For an arbitrarily oriented axis of quantization defined by the Euler angles α, β, γ and the rotation matrix $D^l(\alpha\beta\gamma)$, we have [44] $Y_{lm}(\hat{\mathbf{r}}') = \sum_{m'} D^l_{m'm}(\alpha\beta\gamma) Y_{lm'}(\hat{\mathbf{r}})$. The remaining terms in the matrix element $T_{m,n}$ are invariant with respect to the rotation by these Euler angles. In $\sum_m |T_{m,n}|^2 = \sum_m T^*_{m,n} T_{m,n}$ we have the factor $\sum_m D^{l*}_{m'm}(\alpha\beta\gamma) D^l_{m''m}(\alpha\beta\gamma) = \delta_{m'm''}$, due to the orthonormality relation, which proves our statement. The short-range scattering potential is modeled by the double Yukawa potential

$$V_{\rm S}(r) = -\frac{Z}{H} \frac{e^{-r/D}}{r} [1 + (H-1) e^{-Hr/D}], \tag{15}$$

where $H = DZ^{0.4}$, Z is the nuclear charge, and the values of D for various atomic targets are given in [45]. We suppose that the laser field is bichromatic and elliptically polarized, with the electric-field vector

$$\begin{aligned} \mathbf{E}(t) = {} & \frac{E_1}{\sqrt{1+\varepsilon_1^2}} [\hat{\mathbf{e}}_z \sin(r\omega t) - \hat{\mathbf{e}}_x \varepsilon_1 \cos(r\omega t)] \\ & + \frac{E_2}{\sqrt{1+\varepsilon_2^2}} [\hat{\mathbf{e}}_z \sin(s\omega t + \phi) - h\hat{\mathbf{e}}_x \varepsilon_2 \cos(s\omega t + \phi)], \end{aligned} \tag{16}$$

where $\hat{\mathbf{e}}_x$ and $\hat{\mathbf{e}}_z$ are the unit polarization vectors along the x axis and the z axis, respectively; $E_j = I_j^{1/2}$, I_j, and ε_j are the electric-field amplitude, intensity, and ellipticity of the jth field component ($j = 1,2$), respectively; $r\omega$ and $s\omega$ are integer multiples of the fundamental angular frequency ω; ϕ is the relative phase between the two field components; and $h = 1$ for the corotating and $h = -1$ for the counterrotating field components.

III. CLASSICAL ANALYSIS

As we will show in Sec. IV, the plateaus appearing in the energy spectra of the LAR and SLAR processes are characterized by abrupt cutoffs. These cutoffs are related to the maximum energies of the emitted x-ray photons in the process. They can be explained by a classical analysis.

The argument of the exponential function in the first term of the S-matrix element (9) is the semiclassical action for the LAR process. The condition that the first derivative of the semiclassical action over the recombination time t be equal to zero leads to the equation

$$E_{\rm B} + \omega_{\mathbf{K}} = \tfrac{1}{2}[\mathbf{p} + \mathbf{A}(t)]^2. \tag{17}$$

Equation (17) is the energy-conserving condition at the recombination time t. It can be used to calculate $\omega_{\mathbf{K}}$ for specified values of t.

The argument of the exponential function in the second term of the S-matrix element (9) is the semiclassical action for the SLAR process. The conditions that the first derivatives of the semiclassical action over the recombination time t and the travel time τ be equal to zero provide the equations

$$[\mathbf{k}_{\rm s} + \mathbf{A}(t-\tau)]^2 = [\mathbf{p} + \mathbf{A}(t-\tau)]^2, \tag{18}$$

$$E_{\rm B} + \omega_{\mathbf{K}} = \tfrac{1}{2}[\mathbf{k}_{\rm s} + \mathbf{A}(t)]^2. \tag{19}$$

Equations (18) and (19) are the energy-conserving conditions at the scattering time $t - \tau$ and at the recombination time t, respectively. This system of two nonlinear equations can be solved for t and τ by numerical methods. In this way, we can calculate the emitted x-ray energy $\omega_{\mathbf{K}}$ for different values of the travel time τ.

IV. NUMERICAL RESULTS

In all our calculations, we assume that the incident electron momentum $\mathbf{p}$ is in the laser-field polarization plane (i.e., in the xz plane) and that the wave vector of the emitted x rays $\mathbf{K}$ is perpendicular to the laser-field polarization plane (i.e., along the y axis). The incident electron angle θ is the angle between the z axis and the incident electron momentum. The geometry used in our calculations is presented in Fig. 1. We also assume that the ellipticities and intensities of the two field components are equal ($\varepsilon_1 = \varepsilon_2 = \varepsilon$ and $I_1 = I_2 = I$) and that the relative phase between the field components is $\phi = 0$. We consider the case of the counterrotating field components ($h = -1$).

A. Direct recombination

We first analyze the direct recombination of electrons with ionic targets (LAR). This process is described by the first term on the right-hand side of Eqs. (6) and (10). In Fig. 2 the differential power spectrum for the laser-assisted radiative recombination of electrons with simulated Ar^+ ions is presented as a function of the emitted x-ray energy. The recombination occurs in a bichromatic elliptically polarized laser field having a fundamental wavelength of 800 nm and an intensity of 1.5×10^{15} W/cm^2. The ellipticity of the laser-field components is $\varepsilon = 0.1$.

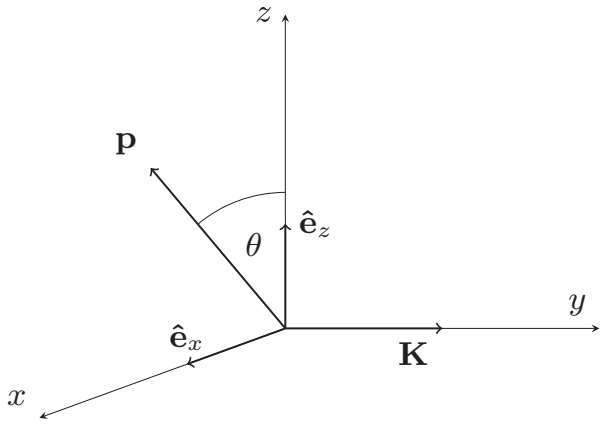

FIG. 1. Geometry of the electron-ion recombination process.

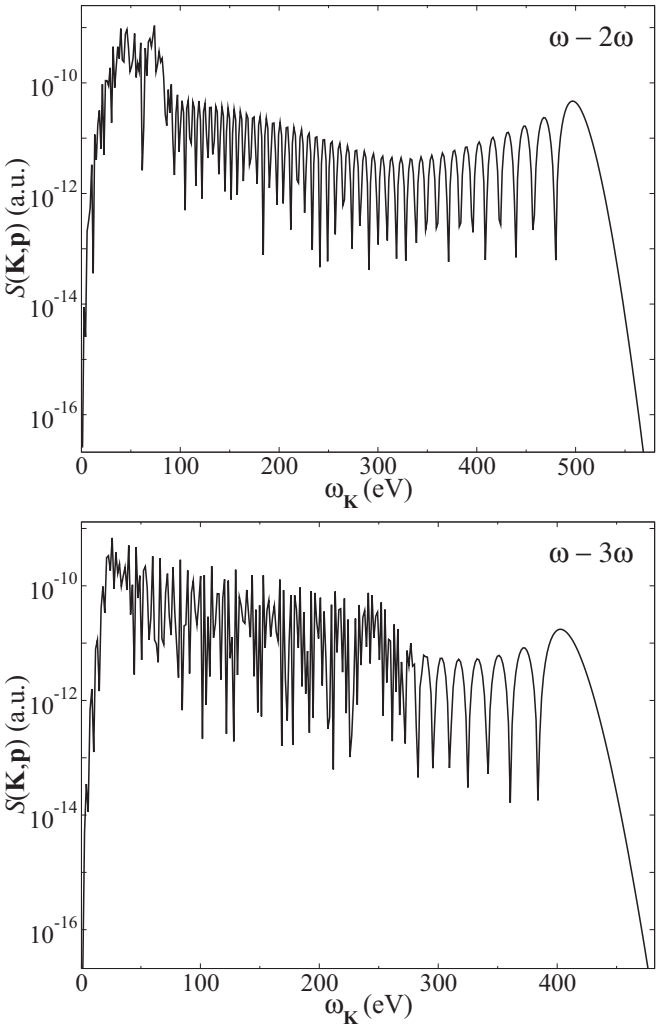

FIG. 2. Differential power spectrum for the laser-assisted radiative recombination of electrons with simulated Ar^+ ions in the presence of a bichromatic elliptically polarized laser field, as a function of the emitted x-ray energy. Only the direct recombination (LAR) is included. The incident electron energy is $E_{\mathbf{p}} = 5$ eV and the incident electron angle is $\theta = 0^\circ$. The fundamental wavelength and the intensity of the laser field are 800 nm and 1.5×10^{15} W/cm^2, respectively. The ellipticity of the laser-field components is $\varepsilon = 0.1$. The results for the ω-2ω ($r = 1, s = 2$) and ω-3ω ($r = 1, s = 3$) fields are presented, as denoted in each panel.

The combination of the angular frequencies of the field components [$r\omega$ and $s\omega$ in Eq. (16)] is denoted in each panel of Fig. 2. The incident electron energy is $E_{\mathbf{p}} = 5$ eV and the incident electron angle is $\theta = 0^\circ$. A plateau that ends with an abrupt cutoff may be seen in both energy spectra presented in Fig. 2. The low-energy part of the plateau has a dense and irregular oscillatory structure. The oscillations in the high-energy part of the plateau are more regular and less intense. The plateau obtained for the ω-3ω field is much richer with oscillations than that obtained for the ω-2ω field. Irregular and dense oscillations end at approximately 90 eV for the ω-2ω case, while such oscillations dominate the plateau up to 260 eV for the ω-3ω case. The oscillatory structures and cutoffs of the plateaus in energy spectra presented in Fig. 2 can be explained by the classical analysis of the direct recombination. Using Eq. (17) for the parameters of Fig. 2, we have calculated the emitted x-ray energy $\omega_{\mathbf{K}}$ as a function of the recombination time t, expressed in laser-field periods T. The results are presented in Fig. 3, which clearly shows that more classical solutions exist for the ω-3ω field than for the ω-2ω field in the middle-energy region (90 eV $< \omega_{\mathbf{K}} <$ 260 eV). More precisely, there are four classical solutions for the ω-3ω field, compared with only two classical solutions for the ω-2ω field in the above-mentioned energy region. As one can see from Fig. 3, the number of contributing solutions decreases with an increase of the emitted x-ray energy. In the high-energy region, close to the plateau cutoff, just two solutions remain. The highest maximum in each panel of Fig. 3 matches the cutoff energy of the plateau in the corresponding panel of Fig. 2. This confirms that the results obtained by numerical integration of the T matrix [Eqs. (10), (11), and (14)] agree very well with the estimates of the classical analysis [Eq. (17)]. One can also notice from Fig. 3 that the x-ray energy is high in relevant regions (from 80–100 eV to 400–500 eV in the cutoff region). If the variables t/T and $\omega_{\mathbf{K}}$ in the horizontal and vertical axes of Fig. 3 are changed to $(t-\tau)/T$ and $\omega_{\mathbf{K}} + E_{\mathrm{B}}$, respectively, then we have the energy of the scattering electrons in the SLAR process [see Eqs. (17) and (18)] as a function of the scattering time $t - \tau$, expressed in laser-field periods. This means that the energy of the scattering electrons in the SLAR process is also high in relevant regions and the Born approximation can be applied.

Another example of the direct recombination energy spectrum is presented in Fig. 4. The incident electron angle is $\theta = 90^\circ$, while the other parameters are the same as in Fig. 2. One can see from Fig. 4 that the oscillatory structure of the low-energy part of the spectrum is very similar to that in Fig. 2, for both the ω-2ω and the ω-3ω field. The high-energy part of the spectrum is also similar to that in Fig. 2 for the ω-2ω field. However, the high-energy parts of the spectra presented in Figs. 2 and 4 are different for the ω-3ω field. While the density of the oscillations decreases beyond 260 eV for $\theta = 0^\circ$ (bottom panel of Fig. 2), the dense and irregular oscillations dominate the entire energy spectrum, including the plateau cutoff, for $\theta = 90^\circ$ (bottom panel of Fig. 4). The explanation of the energy spectrum structure for $\theta = 90^\circ$ is provided by the

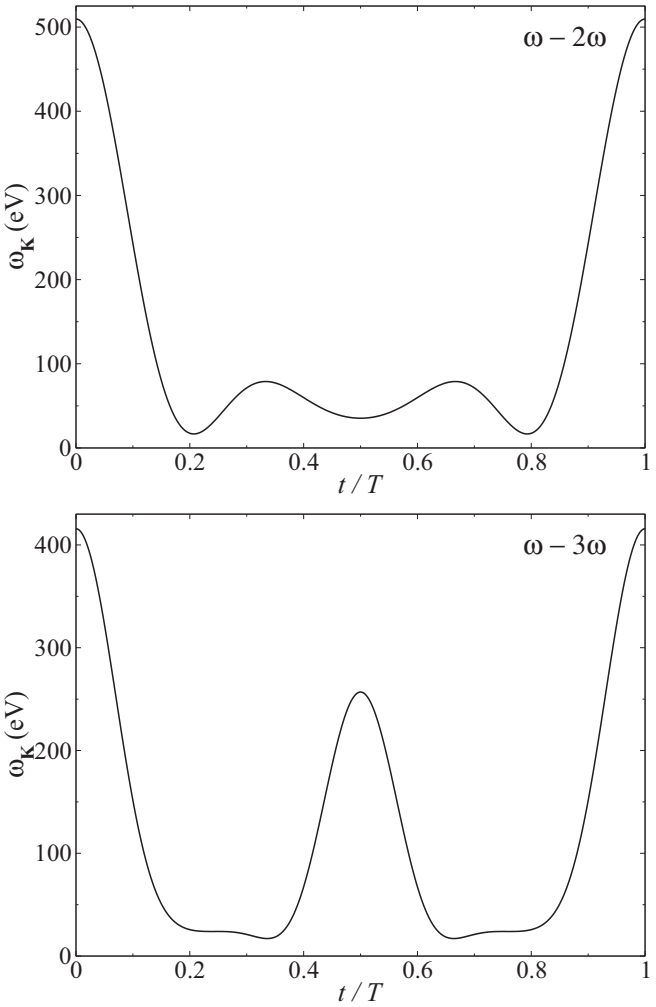

FIG. 3. Classical analysis of the direct recombination solutions for the parameters of Fig. 2. The emitted x-ray energy $\omega_{\mathbf{K}}$ is presented as a function of the recombination time t, expressed in laser-field periods T. The results for the ω-2ω ($r = 1, s = 2$) and ω-3ω ($r = 1, s = 3$) fields are presented, as denoted in each panel.

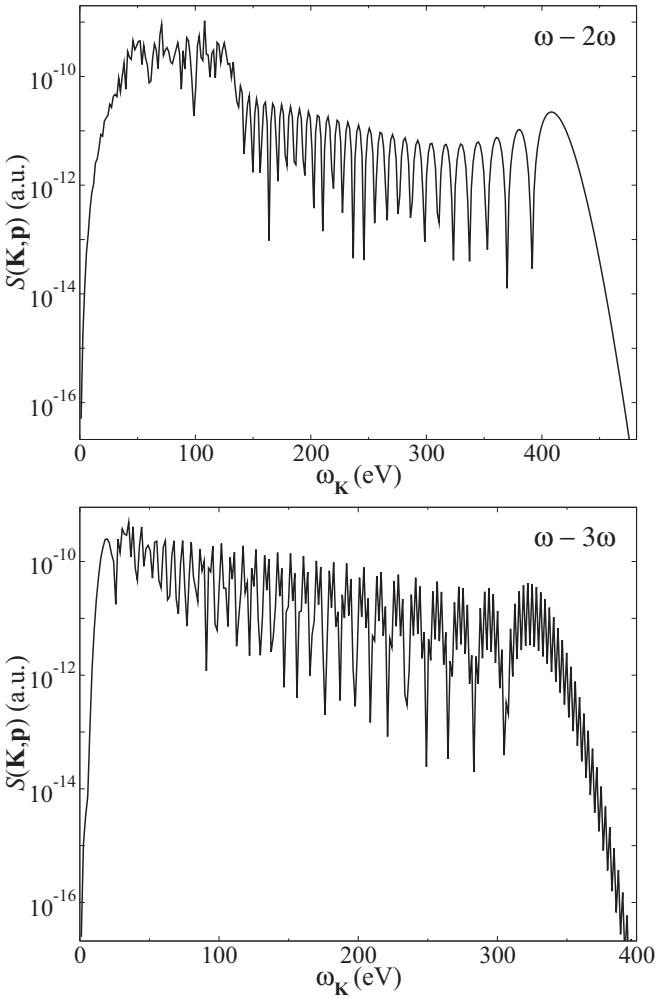

FIG. 4. Same as in Fig. 2, except that the incident electron angle is $\theta = 90^\circ$.

classical analysis, the results of which are presented in Fig. 5. The top panel of Fig. 5 shows that only two classical solutions exist for the ω-2ω field in the high-energy part of the spectrum, while, according to the bottom panel of Fig. 5, four classical solutions exist for the ω-3ω field in the high-energy part of the spectrum, up to the cutoff energy (i.e., the maximum value of the energy).

The oscillatory structures in the recombination energy spectra are a consequence of the interference of classical solutions. The oscillatory maxima (minima) in the energy spectra are related to the constructive (destructive) interference of classical solutions. The larger the number of classical solutions, the denser and more irregular the oscillations are. The classical solutions represent the classical trajectories of the electron in the laser field. These trajectories are characterized by the recombination time t. They offer an alternative way to calculate the differential power spectrum as a function of the emitted x-ray energy. We will briefly explain it. Instead of numerical integration over the time t in Eq. (11), the T-matrix element may be expressed as a sum over the stationary points t_s [46]. These stationary points are actually the above-mentioned classical solutions, i.e., the solutions of Eq. (17). For a given value of the emitted x-ray energy, there is a certain number of stationary points t_s. Each of these stationary points gives a contribution to the T-matrix element. The interference of these contributions is responsible for the oscillations in the energy spectrum. The described procedure is called the stationary phase method and is based on Feynman's path-integral interpretation of quantum physics, which states that the probability amplitude of a quantum-mechanical process can be represented as a coherent superposition of all possible spatiotemporal paths that connect the initial and the final state of the system [47,48].

B. Recombination preceded by scattering

We now investigate the scattering effects that may occur in the process of the laser-assisted electron-ion recombination. In the following calculations, both the LAR (direct recombination) and SLAR (recombination preceded by a scattering) are included. The SLAR process is described by the second term on the right-hand side of Eqs. (6) and (10). The recombination

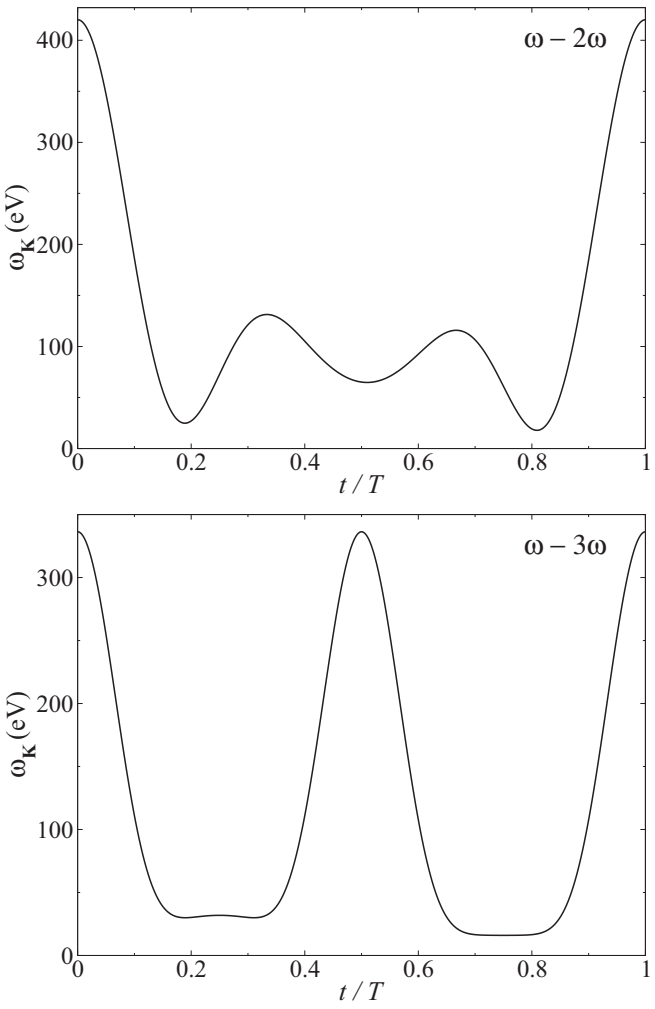

FIG. 5. Classical analysis of the direct recombination solutions for the parameters of Fig. 4. The notation is the same as in Fig. 3.

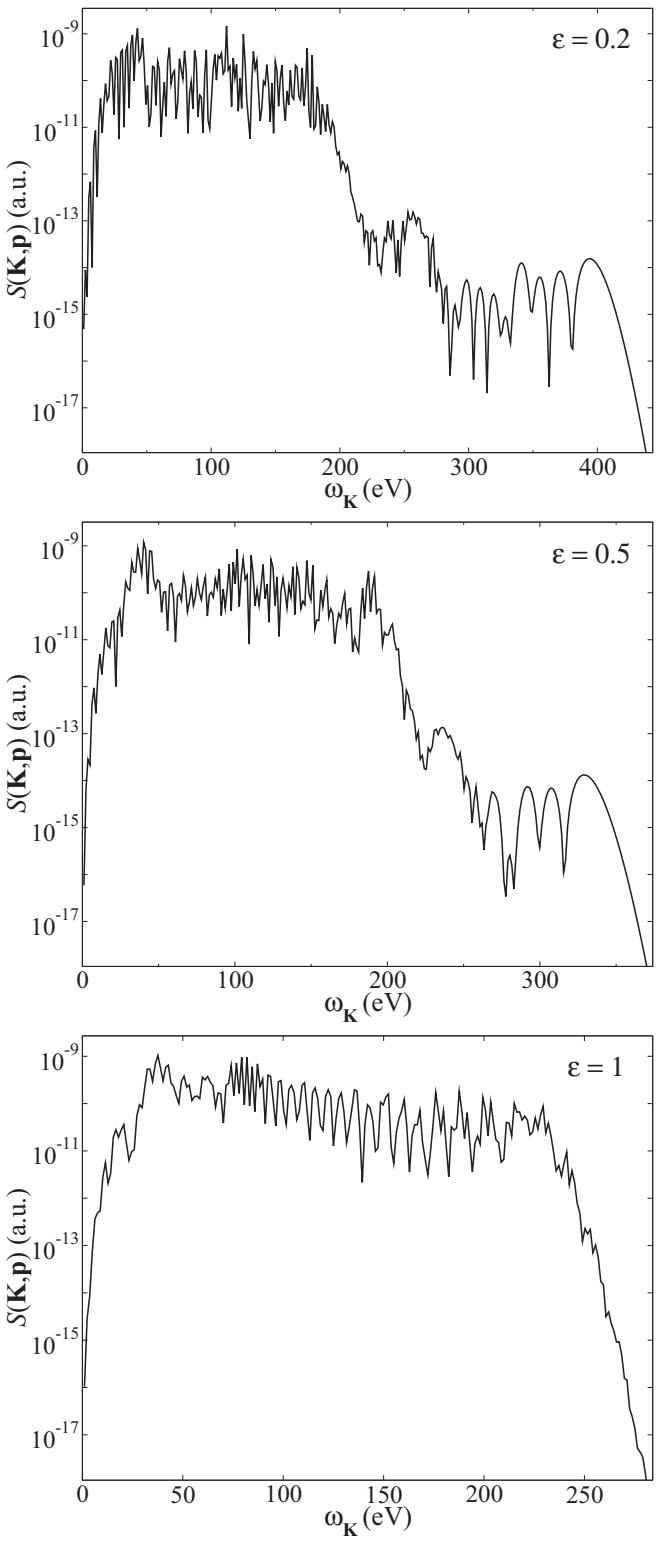

FIG. 6. Differential power spectrum for the laser-assisted radiative recombination of electrons with simulated Kr^+ ions in the presence of a bichromatic elliptically polarized ω-2ω ($r = 1, s = 2$) laser field, as a function of the emitted x-ray energy. Both the LAR and SLAR processes are included. The incident electron energy is $E_{\mathbf{p}} = 15$ eV and the incident electron angle is $\theta = 180^\circ$. The fundamental wavelength and the intensity of the laser field are 950 nm and 8×10^{14} W/cm^2, respectively. The ellipticity of the laser-field components is denoted in each panel.

energy spectra depend on the laser-field and incident electron parameters. They also depend on the type of ionic target. We will first illustrate how the ellipticity of the laser-field components affects the recombination energy spectra. The results are shown in Fig. 6, where the differential power spectrum for the laser-assisted radiative recombination of electrons with simulated Kr^+ ions is presented as a function of the emitted x-ray energy. The incident electron energy and angle are $E_{\mathbf{p}} = 15$ eV and $\theta = 180^\circ$, respectively. The fundamental wavelength and the intensity of the bichromatic elliptically polarized laser field are 950 nm and 8×10^{14} W/cm^2, respectively. The angular frequencies of the laser-field components are ω and 2ω, where ω is the fundamental angular frequency. The ellipticity of the laser-field components is denoted in each panel of Fig. 6. The results presented in Fig. 6 lead to the conclusion that plateaus in the energy spectra depend on the ellipticity of the laser-field components. There are two plateaus in the energy spectra for $\varepsilon = 0.2$ and $\varepsilon = 0.5$. The first plateau appears in the low-energy part of the spectrum and represents LAR, while the second one appears in the high-energy part of the spectrum and is a consequence of SLAR. The first plateau is considerably higher than the second one, because the probability of the

LAR process is much higher than that of the SLAR process. As the ellipticity of the laser field is increased, the cutoff of the higher (LAR) plateau slowly shifts to higher energy values, while the cutoff energy of the lower (SLAR) plateau decreases. It is clearly visible that the shrinking of the SLAR plateau is faster than the expanding of the LAR plateau as the ellipticity of the laser field increases. For high ellipticity values, the cutoff energy of the LAR plateau is higher than that of the SLAR plateau, so the SLAR plateau is completely masked by the LAR plateau. This can be seen from the bottom panel of Fig. 6, where the results for $\varepsilon = 1$ are presented.

The recombination energy spectra are also dependent on the incident electron angle. This is illustrated in Fig. 7, where the differential power spectrum for the laser-assisted radiative recombination of electrons with simulated Ar^+ ions is presented as a function of the emitted x-ray energy. The process occurs in a bichromatic elliptically polarized laser field having a fundamental wavelength of 950 nm and an intensity of 10^{15} W/cm^2. The ellipticity of the laser-field components is $\varepsilon = 0.2$, while the angular frequencies of the components are the same as in Fig. 6. The incident electron energy is $E_{\mathbf{p}} = 10$ eV. The incident electron angle θ is denoted in each panel of Fig. 7. One can see from Fig. 7 that the cutoff energy of the higher (LAR) plateau significantly decreases with the increase of the angle θ, while the cutoff energy of the lower (SLAR) plateau remains practically unchanged when θ is varied (compare the results for $\theta = 90^\circ$ and $\theta = 180^\circ$, presented in the middle and the bottom panel of Fig. 7, respectively). Such a behavior of the plateau cutoffs in the recombination spectra is verified by our classical analysis. The results of the classical analysis are shown in Fig. 8, where the maximum value of the emitted x-ray energy is presented as a function of the incident electron angle θ. Figure 8 confirms that the SLAR plateau is completely masked by the LAR plateau for small values of the angle θ. One can also see from Fig. 8 that the cutoff energy of the LAR plateau steeply decreases with the increase of the angle θ, while the cutoff energy of the SLAR plateau just slightly varies with θ.

Let us analyze the influence of the incident electron energy on the plateaulike structures that appear in the recombination energy spectra. In Fig. 9 the differential power spectrum for the laser-assisted radiative recombination of electrons with simulated He^+ ions is presented as a function of the emitted x-ray energy. The process is assisted by a bichromatic elliptically polarized laser field having a fundamental wavelength of 800 nm and an intensity of 2×10^{15} W/cm^2. The ellipticity of the laser-field components is $\varepsilon = 0.1$ and the incident electron angle is $\theta = 90^\circ$. The angular frequencies of the laser-field components are ω and 3ω, where ω is the fundamental angular frequency. The results for incident electron energies of 5, 25, and 150 eV are presented in the top, middle, and bottom panels of Fig. 9, respectively. The entire LAR plateau shifts to higher energies in the recombination spectrum with the increase of the incident electron energy. In other words, both the minimum and the maximum value of the emitted x-ray energy in the LAR process increase as the incident electron energy increases. The SLAR plateau in the high-energy part of the spectrum is visible if the incident electron energy is low enough. This is illustrated in the top and middle panels of Fig. 9, where the results

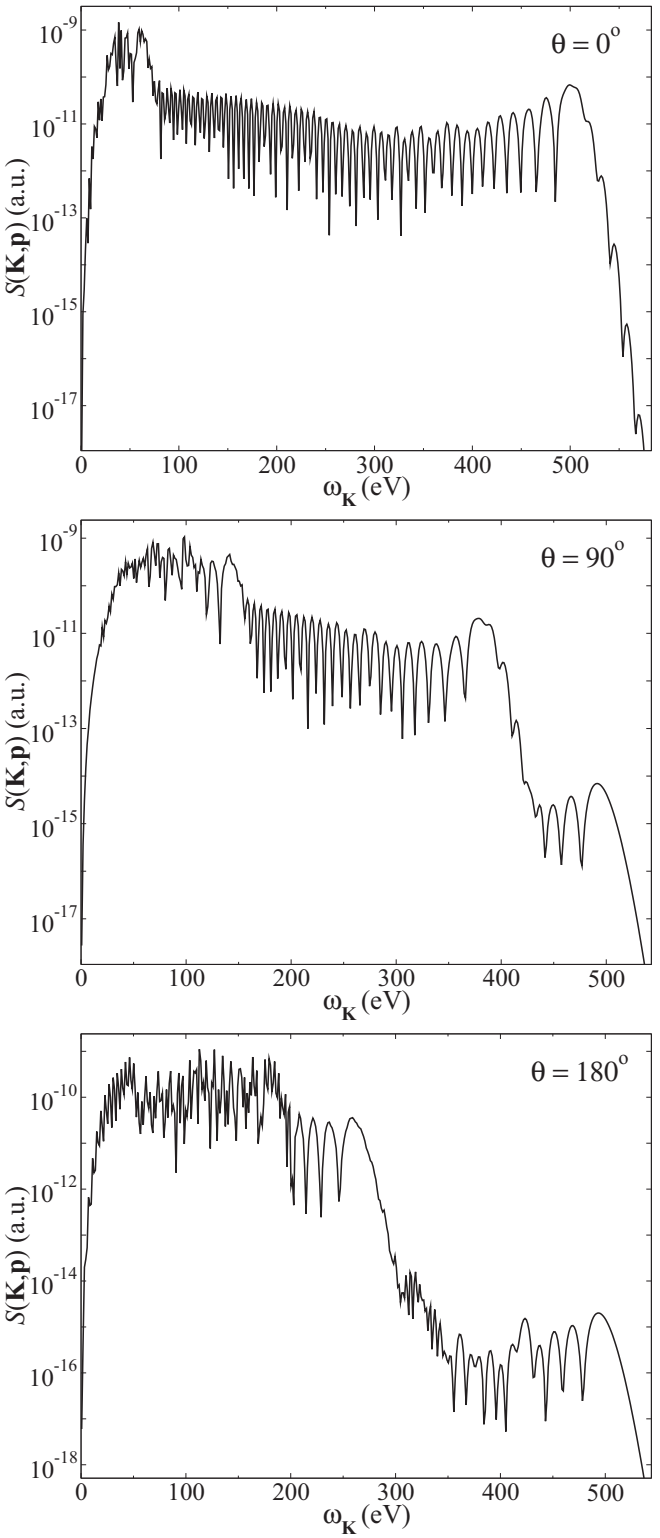

FIG. 7. Differential power spectrum for the laser-assisted radiative recombination of electrons with simulated Ar^+ ions in the presence of a bichromatic elliptically polarized ω-2ω ($r = 1, s = 2$) laser field, as a function of the emitted x-ray energy. Both the LAR and SLAR processes are included. The incident electron energy is $E_{\mathbf{p}} = 10$ eV. The fundamental wavelength and the intensity of the laser field are 950 nm and 10^{15} W/cm^2, respectively. The ellipticity of the laser-field components is $\varepsilon = 0.2$, while the incident electron angle θ is denoted in each panel.

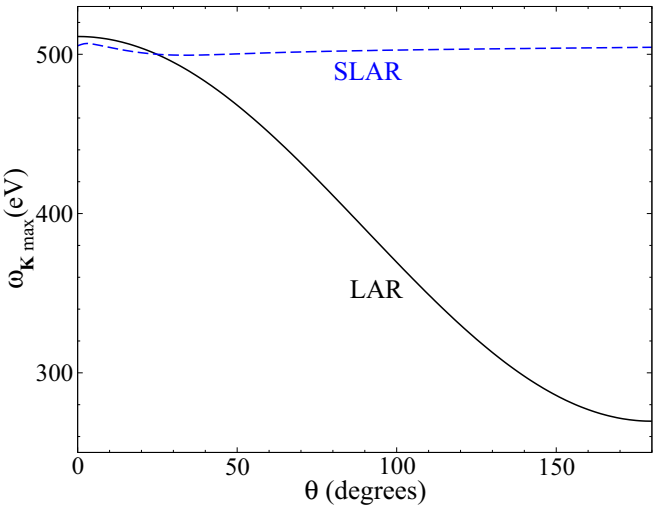

FIG. 8. Classical results for the maximum value of the emitted x-ray energy in the electron–simulated-Ar^+-ion radiative recombination process as a function of the incident electron angle θ. The laser-field parameters and the incident electron energy are the same as in Fig. 7. The results for LAR (solid black line) and SLAR (dashed blue line) are presented.

for $E_{\mathbf{p}} = 5$ eV and $E_{\mathbf{p}} = 25$ eV are respectively presented. The SLAR plateau in the high-energy part of the spectrum is approximately six orders of magnitude lower than the LAR plateau. For high values of the incident electron energy, the SLAR plateau is completely masked by the LAR plateau in the high-energy part of the recombination spectrum. On the other hand, the shifting of the LAR plateau to higher energies in the recombination spectrum unmasks the SLAR plateau in the low-energy part of the spectrum, as one can see from the bottom panel of Fig. 9, where the results for $E_{\mathbf{p}} = 150$ eV are presented. One can also notice that the low-energy part of the SLAR plateau is by one order of magnitude higher than the high-energy part of the same plateau. This may be explained by the fact that more classical solutions for the SLAR process exist in the low-energy region than in the high-energy region. All classical solutions contribute to the T-matrix element and the differential power spectrum is a coherent sum of these solutions.

The plateaus in the recombination energy spectra are also sensitive to the laser-field intensity. We illustrate this in Fig. 10, where the differential power spectrum for the laser-assisted radiative recombination of electrons with simulated Ne^+ ions is presented as a function of the emitted x-ray energy. The incident electron energy and angle are $E_{\mathbf{p}} = 5$ eV and $\theta = 180^\circ$, respectively. The fundamental wavelength of the bichromatic elliptically polarized laser field is 800 nm. The ellipticity of the laser-field components is $\varepsilon = 0.1$, while the angular frequencies of the components are the same as in Figs. 6 and 7. The results for the laser-field intensities of 2×10^{14}, 5×10^{14}, and 10^{15} W/cm^2 are presented in the top, middle, and bottom panels of Fig. 10, respectively. As one can see from Fig. 10, the cutoff energy (i.e., the maximum energy of the emitted x rays) of the both plateaus increases with the increase of the laser-field intensity. It is also visible that the cutoff energy of the SLAR plateau increases faster than that

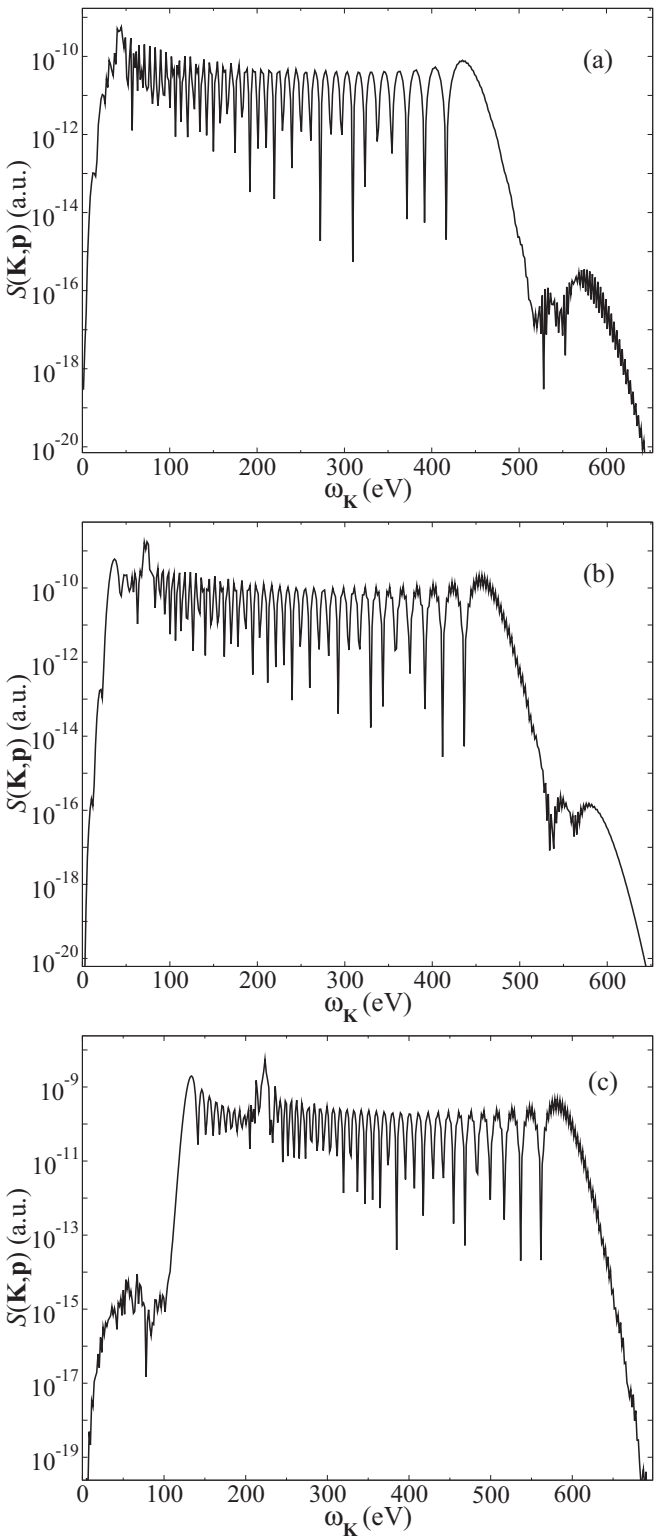

FIG. 9. Differential power spectrum for the laser-assisted radiative recombination of electrons with simulated He^+ ions in the presence of a bichromatic elliptically polarized ω-3ω ($r = 1, s = 3$) laser field, as a function of the emitted x-ray energy. Both the LAR and SLAR processes are included. The fundamental wavelength and the intensity of the laser field are 800 nm and 2×10^{15} W/cm^2, respectively. The ellipticity of the laser-field components is $\varepsilon = 0.1$. The incident electron angle is $\theta = 90^\circ$, while the incident electron energies are (a) $E_{\mathbf{p}} = 5$ eV, (b) $E_{\mathbf{p}} = 25$ eV, and (c) $E_{\mathbf{p}} = 150$ eV.

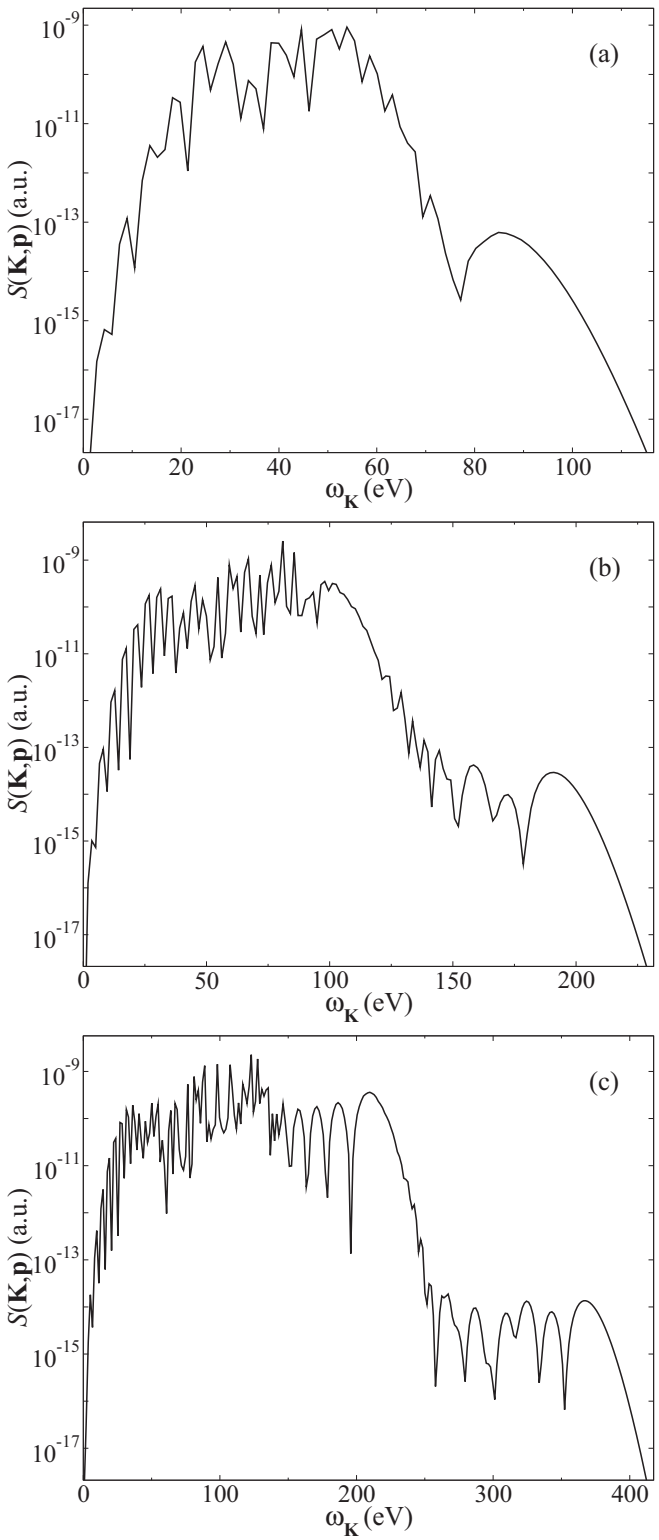

FIG. 10. Differential power spectrum for the laser-assisted radiative recombination of electrons with simulated Ne^+ ions in the presence of a bichromatic elliptically polarized ω-2ω ($r = 1, s = 2$) laser field, as a function of the emitted x-ray energy. Both the LAR and SLAR processes are included. The incident electron energy is $E_{\mathbf{p}} = 5$ eV and the incident electron angle is $\theta = 180^\circ$. The fundamental wavelength of the laser field is 800 nm and the ellipticity of the laser-field components is $\varepsilon = 0.1$. The intensities of the laser field are (a) 2×10^{14} W/cm^2, (b) 5×10^{14} W/cm^2, and (c) 10^{15} W/cm^2.

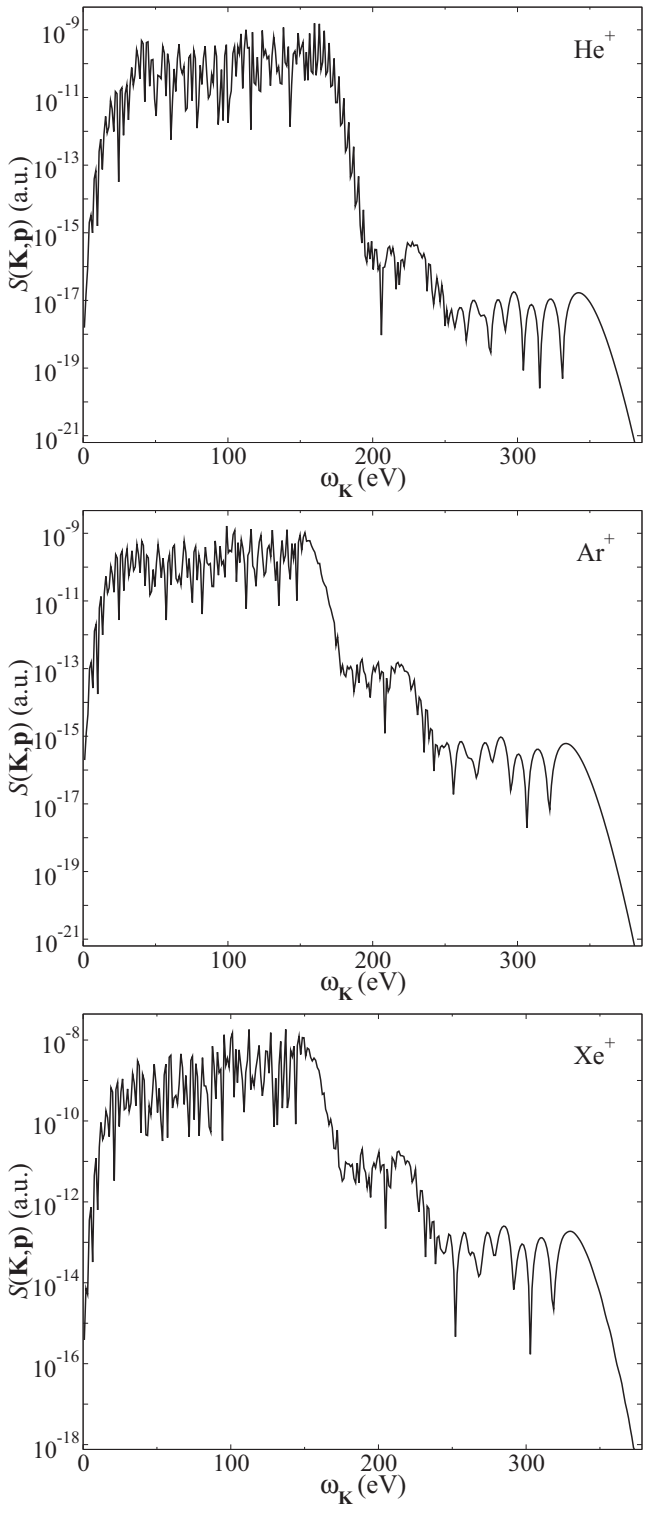

FIG. 11. Differential power spectrum for the laser-assisted radiative recombination of electrons with simulated He^+ (top panel), Ar^+ (middle panel), and Xe^+ (bottom panel) ions in the presence of a bichromatic elliptically polarized ω-2ω ($r = 1, s = 2$) laser field, as a function of the emitted x-ray energy. Both the LAR and SLAR processes are included. The incident electron energy is $E_{\mathbf{p}} = 15$ eV and the incident electron angle is $\theta = 180^\circ$. The fundamental wavelength and the intensity of the laser field are 1100 nm and 5×10^{14} W/cm^2, respectively. The ellipticity of the laser-field components is $\varepsilon = 0.2$.

of the LAR plateau when the laser-field intensity is increased. We conclude that the SLAR plateau is more pronounced at higher intensities of the laser field.

Recombination energy spectra for different ionic targets are presented in Fig. 11, where the differential power spectrum for the laser-assisted radiative recombination of electrons with simulated He^+, Ar^+, and Xe^+ ions is presented as a function of the emitted x-ray energy. The electron-ion recombination is assisted by a bichromatic elliptically polarized laser field having a fundamental wavelength of 1100 nm and an intensity of 5×10^{14} W/cm^2. The incident electron energy and angle are $E_{\mathbf{p}} = 15$ eV and $\theta = 180^\circ$, respectively. The ellipticity of the laser field components is $\varepsilon = 0.2$ and the angular frequencies of the components are the same as in Figs. 6, 7, and 10. The maximum value of the emitted x-ray energy slightly depends on the type of the ionic target, as different ions have different values of the binding energy E_{B}. This is confirmed by Fig. 11, which shows that the cutoff energy of both the LAR and SLAR plateaus is almost unaffected by the type of the ionic target. However, the type of the ionic target strongly affects the value of the differential power spectrum, i.e., the heights of the plateaus in the recombination energy spectrum. It is interesting to note that the difference between the heights of the LAR and the SLAR plateau is smaller for heavier ionic targets. The heavier the ionic target, the smaller the difference in height between the LAR and the SLAR plateau in the energy spectrum, as Fig. 11 clearly shows. While the height of the LAR plateau is only slightly affected by the mass and size of the ionic target, the height of the SLAR plateau is considerably increased when more massive and bigger ionic targets are used. For example, the comparison of the top panel and the bottom panel of Fig. 11 shows that the LAR plateau for the electron–simulated-Xe^+-ion recombination is by one order of magnitude higher than that for the electron–simulated-He^+-ion recombination, while the SLAR plateau for the electron–simulated-Xe^+-ion recombination is by four orders of magnitude higher than that for the electron–simulated-He^+-ion recombination. This behavior of the plateaus in the recombination energy spectra for different ionic targets can be explained by the fact that bigger and heavier targets have more scattering centers, so the probability of the SLAR process (which includes scattering) is increased. The results presented in Fig. 11 lead to the conclusion that the process of the laser-assisted electron-ion recombination, especially the recombination preceded by a scattering, can be enhanced by the use of heavier ionic targets.

We now comment on the role of the scattering potential. The short-range potential (15) that we used in our calculations is an approximation to the real electron-ion scattering potential. A better approximation is the potential

$$V(r) = -\frac{1 + a_1 e^{-a_2 r} + a_3 r e^{-a_4 r} + a_5 e^{-a_6 r}}{r} \qquad (20)$$

that supports atomic bound states. The coefficients a_i ($i = 1,2,\ldots,6$) for various atomic and ionic targets may be found in Refs. [49,50]. The first term on the right-hand of Eq. (20) is the Coulomb potential $-1/r$. Its Fourier transform is proportional to $1/(\mathbf{p}-\mathbf{k}_{\mathrm{s}})^2$. As $\mathbf{k}_{\mathrm{s}}$ is a function of t and τ and we integrate over t and τ when calculating the T-matrix element (11), it is

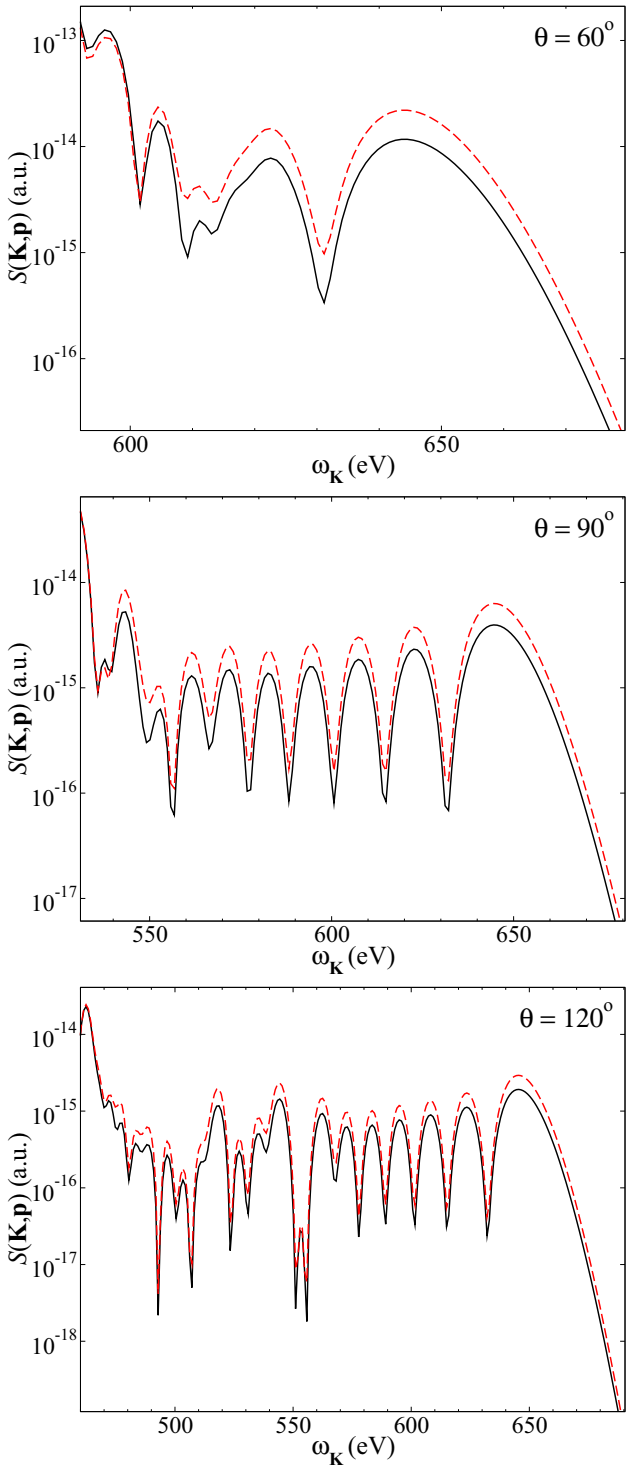

FIG. 12. Differential power spectrum for the laser-assisted radiative recombination of electrons with simulated Ar^+ ions in the presence of a bichromatic elliptically polarized ω-2ω ($r = 1, s = 2$) laser field, as a function of the emitted x-ray energy. The incident electron energy is $E_{\mathbf{p}} = 10$ eV. The fundamental wavelength and the intensity of the laser field are 1300 nm and 7×10^{14} W/cm^2, respectively. The ellipticity of the laser-field components is $\varepsilon = 0.2$, while the incident electron angle θ is denoted in each panel. The results calculated with the potentials (15) (solid black line) and (20) (dashed red line) are presented.

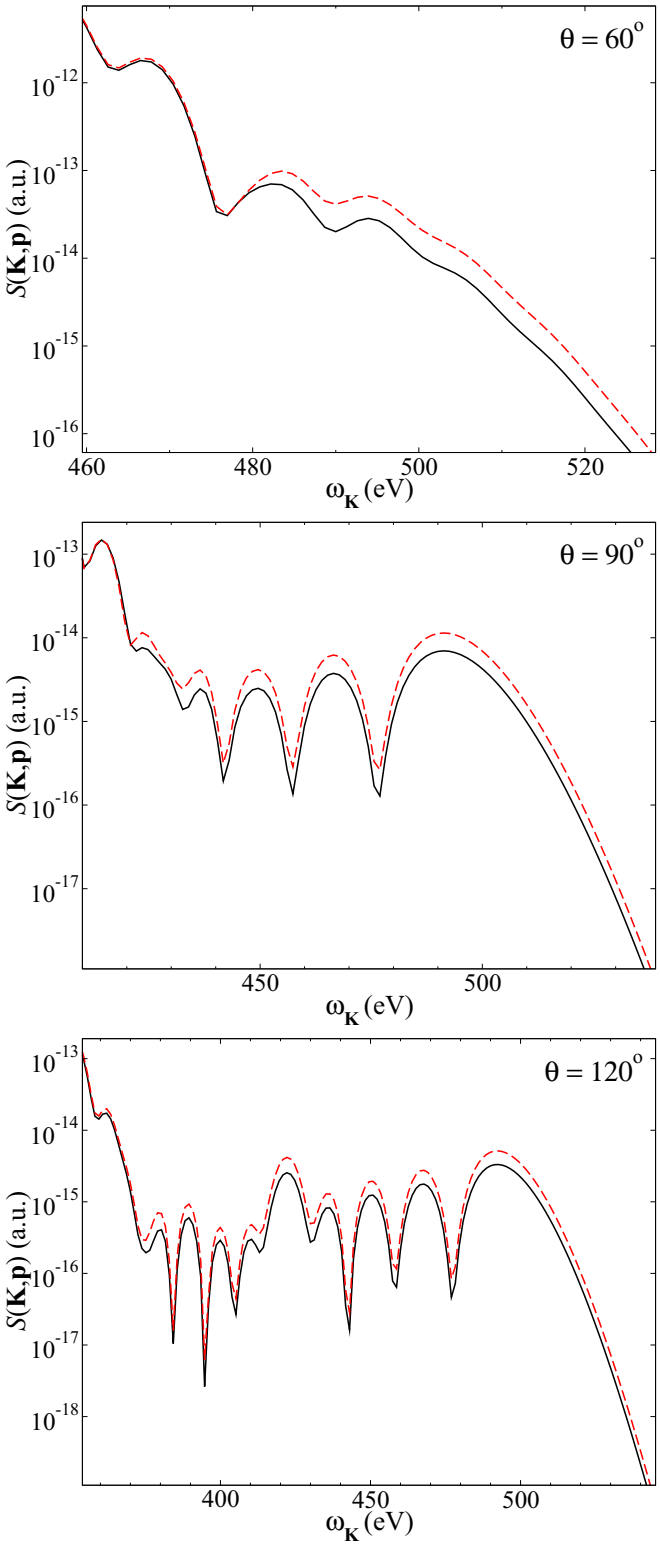

FIG. 13. Differential power spectrum for the laser-assisted radiative recombination of electrons with simulated Ar^+ ions in the presence of a bichromatic elliptically polarized ω-2ω ($r = 1, s = 2$) laser field, as a function of the emitted x-ray energy. The incident electron angle θ is denoted in each panel, while the other parameters are the same as in Fig. 7. The results calculated with the potentials (15) (solid black line) and (20) (dashed red line) are presented.

possible that the Fourier transform of the Coulomb potential diverges for certain values of t and τ when the incident electron angle θ is close to 0° and 180°. In order to avoid this problem, we have used the short-range potential (15) in our calculations. We will now show that approximating the scattering potential with the short-range potential (15) is justified. A comparison of the results that are calculated with the potentials (15) and (20) is illustrated in Fig. 12, where the differential power spectrum for the laser-assisted radiative recombination of electrons with simulated Ar^+ ions is presented as a function of the emitted x-ray energy. The fundamental wavelength and the intensity of the bichromatic elliptically polarized laser field are 1300 nm and 7×10^{14} W/cm^2, respectively. The ellipticity of the laser-field components is $\varepsilon = 0.2$, while the angular frequencies of the components are the same as in Figs. 6, 7, 10, and 11. The incident electron energy is $E_{\mathbf{p}} = 10$ eV. The incident electron angle θ is denoted in each panel of Fig. 12. Only the high-energy region (i.e., the SLAR plateau), where the scattering effects are noticeable, is presented in Fig. 12. A similar comparison is shown in Fig. 13, but for the parameters of Fig. 7. One can notice that the results calculated with the potentials (15) and (20) are in good agreement for the chosen incident electron and laser beam parameters.

V. CONCLUSION

The plateaulike structures with abrupt cutoffs are a general feature of the energy spectra of atomic and molecular processes in strong laser fields. These plateaus are formed by a series of oscillatory minima and maxima in the energy spectrum. The possibility of experimental observation of the plateaus in the energy spectra depends on the particular process. The plateaus in the energy spectra of laser-induced processes, such as above-threshold ionization, above-threshold detachment, and high-order-harmonic generation, have been experimentally observed. On the other hand, there is no experimental confirmation of the existence of the plateaus in the energy spectra of laser-assisted processes, such as electron-ion recombination and electron-atom scattering. This is due to the low counting rates in the so-called three-beam experiments that must be performed in order to observe these processes.

We have presented the S-matrix theory of the electron-ion radiative recombination assisted by a bichromatic elliptically polarized laser field. We have analyzed the first-order (LAR) and the second-order process (SLAR), both of which are characterized by a plateau in the energy spectrum. Our theory includes a recombination of electrons in the s ($l = 0$ for He) and p ($l = 1$ for Ne, Ar, Kr, and Xe) atomic ground states. The quantum-mechanical results have been verified by a classical analysis. Our calculations show that the differential power spectrum of the laser-assisted electron-ion recombination is very low, especially for the SLAR process. The value of the differential power spectrum can be increased by choosing heavier and bigger ionic targets. Therefore, it would be interesting to investigate the recombination of electrons with molecular ions. We have also illustrated that the plateau structures in the recombination energy spectra depend on the incident electron and laser-field parameters. In particular, the

cutoff energy of the plateaus is a function of the incident electron energy and angle, and the intensity and ellipticity of the laser field. The cutoff energies of the LAR and SLAR processes increase with increasing intensity of the laser field. The length of the plateaus in the energy spectra also varies with the ellipticity of the laser field. While the cutoff energy of the LAR plateau increases, the cutoff energy of the SLAR plateau decreases with increasing ellipticity of the laser field. Finally, it is interesting to note that the low-energy part of the SLAR plateau becomes visible for higher values of the incident electron energy. This effect is particularly pronounced for the ω-3ω combination of the angular frequencies of the laser-field components.

ACKNOWLEDGMENT

This work was supported in part by the Deutsche Forschungsgemeinschaft within the Priority Programme Quantum Dynamics in Tailored Intense Fields.

[1] L. F. DiMauro and P. Agostini, Adv. At. Mol. Opt. Phys. **35**, 79 (1995).
[2] M. Protopapas, C. H. Keitel, and P. L. Knight, Rep. Prog. Phys. **60**, 389 (1997).
[3] C. J. Joachain, M. Dörr, and N. Kylstra, Adv. At. Mol. Opt. Phys. **42**, 225 (2000).
[4] P. Salières, A. L'Huilier, P. Antoine, and M. Lewenstein, Adv. At. Mol. Opt. Phys. **41**, 83 (1999).
[5] T. Brabec and F. Krausz, Rev. Mod. Phys. **72**, 545 (2000).
[6] W. Becker, F. Grasbon, R. Kopold, D. B. Milošević, G. G. Paulus, and H. Walther, Adv. At. Mol. Opt. Phys. **48**, 35 (2002).
[7] D. B. Milošević and F. Ehlotzky, Adv. At. Mol. Opt. Phys. **49**, 373 (2003).
[8] F. Krausz and M. Ivanov, Rev. Mod. Phys. **81**, 163 (2009).
[9] M. Kohler, T. Pfeifer, K. Hatsagortsyan, and C. Keitel, Adv. At. Mol. Opt. Phys. **61**, 159 (2012).
[10] R. V. Karapetyan and M. V. Fedorov, Zh. Eksp. Teor. Fiz. **75**, 816 (1978) [Sov. Phys. JETP **48**, 412 (1978)].
[11] F. Zhou and L. Rosenberg, Phys. Rev. A **48**, 505 (1993).
[12] F. Ehlotzky, A. Jaroń, and J. Z. Kamiński, Phys. Rep. **297**, 63 (1998).
[13] M. Dondera and V. Florescu, Radiat. Phys. Chem. **75**, 1380 (2006).
[14] A. N. Zheltukhin, A. V. Flegel, M. V. Frolov, N. L. Manakov, and A. F. Starace, Phys. Rev. A **89**, 023407 (2014).
[15] A. N. Zheltukhin, A. V. Flegel, M. V. Frolov, N. L. Manakov, and A. F. Starace, J. Phys. B **48**, 075202 (2015).
[16] D. B. Milošević and F. Ehlotzky, Phys. Rev. A **58**, 2319 (1998).
[17] D. B. Milošević and A. F. Starace, Phys. Rev. Lett. **81**, 5097 (1998); Laser Phys. **10**, 278 (2000).
[18] D. B. Milošević and A. F. Starace, J. Phys. B **32**, 1831 (1999); Phys. Rev. A **60**, 3943 (1999).
[19] A. Jaroń, J. Z. Kamiński, and F. Ehlotzky, Phys. Rev. A **61**, 023404 (2000); **63**, 055401 (2001); Laser Phys. **11**, 174 (2001).
[20] M. Y. Kuchiev and V. N. Ostrovsky, Phys. Rev. A **61**, 033414 (2000); J. Phys. B **34**, 405 (2001) (see Appendix B about LAR in the context of high-order-harmonic generation).
[21] Y. Hahn, Rep. Prog. Phys. **60**, 691 (1997).
[22] C. Leone, S. Bivona, R. Burlon, and G. Ferrante, Phys. Rev. A **66**, 051403 (2002).
[23] S. Bivona, R. Burlon, G. Ferrante, and C. Leone, J. Opt. Soc. Am. B **22**, 2076 (2005).
[24] G. Shchedrin and A. Volberg, J. Phys. A **44**, 245301 (2011).
[25] A. Jaroń, J. Z. Kamiński, and F. Ehlotzky, J. Phys. B **34**, 1221 (2001).
[26] S. Odžak and D. B. Milošević, Phys. Rev. A **92**, 053416 (2015).
[27] J. Z. Kamiński and F. Ehlotzky, Phys. Rev. A **71**, 043402 (2005); J. Mod. Opt. **53**, 7 (2006).
[28] S. Bivona, R. Burlon, G. Ferrante, and C. Leone, Opt. Express **14**, 3715 (2006).
[29] S. Bivona, R. Burlon, and C. Leone, Laser Phys. Lett. **4**, 44 (2007).
[30] D. B. Milošević and F. Ehlotzky, Phys. Rev. A **65**, 042504 (2002); J. Mod. Opt. **50**, 657 (2003).
[31] A. N. Zheltukhin, N. L. Manakov, A. V. Flegel, and M. V. Frolov, Pis'ma Zh. Eksp. Teor. Fiz. **94**, 641 (2011) [JETP Lett. **94**, 599 (2011)].
[32] A. N. Zheltukhin, A. V. Flegel, M. V. Frolov, N. L. Manakov, and A. F. Starace, J. Phys. B **45**, 081001 (2012).
[33] A. Čerkić and D. B. Milošević, Phys. Rev. A **88**, 023414 (2013).
[34] K. R. Overstreet, R. R. Jones, and T. F. Gallagher, Phys. Rev. Lett. **106**, 033002 (2011).
[35] T. Mohamed, G. Andler, M. Fogle, E. Justiniano, S. Madzunkov, and R. Schuch, Phys. Rev. A **83**, 032702 (2011).
[36] U. Schramm, J. Berger, M. Grieser, D. Habs, E. Jaeschke, G. Kilgus, D. Schwalm, A. Wolf, R. Neumann, and R. Schuch, Phys. Rev. Lett. **67**, 22 (1991); A. Scrinzi, N. Elander, and A. Wolf, Z. Phys. D **34**, 185 (1995); U. Schramm, T. Schramm, D. Habs, D. Schwalm, and A. Wolf, Hyperfine Interact. **99**, 309 (1996); U. Schramm, A. Wolf, T. Schüßler, D. Habs, D. Schwalm, O. Uwira, J. Linkemann, and A. Müller, *ibid.* **108**, 273 (1997).
[37] M. L. Rogelstad, F. B. Yousif, T. J. Morgan, and J. B. A. Mitchell, J. Phys. B **30**, 3913 (1997); C. Wesdorp, F. Robicheaux, and L. D. Noordam, Phys. Rev. Lett. **84**, 3799 (2000); G. Gabrielse, Adv. At. Mol. Opt. Phys. **50**, 155 (2005).
[38] R. A. Müller, D. Seipt, S. Fritzsche, and A. Surzhykov, Phys. Rev. A **92**, 053426 (2015).
[39] V. A. Zaytsev, V. G. Serbo, and V. M. Shabaev, Phys. Rev. A **95**, 012702 (2017).
[40] D. B. Milošević and F. Ehlotzky, Phys. Rev. A **57**, 5002 (1998).
[41] D. B. Milošević and F. Ehlotzky, Phys. Rev. A **58**, 3124 (1998); J. Phys. B **31**, 4149 (1998); **32**, 1585 (1999).
[42] D. B. Milošević, Phys. Rev. A **92**, 043827 (2015).
[43] D. B. Milošević and W. Becker, Phys. Rev. A **93**, 063418 (2016).
[44] M. E. Rose, *Elementary Theory of Angular Momentum* (Dover, New York, 1995).

[45] A. E. S. Green, D. L. Sellin, and A. S. Zachor, Phys. Rev. **184**, 1 (1969).
[46] A. Čerkić and D. B. Milošević, Phys. Rev. A **73**, 033413 (2006).
[47] P. Salières, B. Carré, L. Le Déroff, F. Grasbon, G. G. Paulus, H. Walther, R. Kopold, W. Becker, D. B. Milošević, A. Sanpera, and M. Lewenstein, Science **292**, 902 (2001).
[48] D. B. Milošević, D. Bauer, and W. Becker, J. Mod. Opt. **53**, 125 (2006).
[49] X. M. Tong and C. D. Lin, J. Phys. B **38**, 2593 (2005).
[50] D. B. Milošević, W. Becker, M. Okunishi, G. Prümper, K. Shimada, and K. Ueda, J. Phys. B **43**, 015401 (2010).